PROCEEDINGS OF THE INTERNATIONAL SYMPOSIUM ON
INTENSE DYNAMIC LOADING AND ITS EFFECTS
CHENGDU, CHINA, JUNE 9—12, 1992

SHOCK SYNTHESIS OF SILICIDES: MICROSTRUCTURES AND MECHANISMS

Li-Hsing Yu+, Marc A. Meyers*, and Kenneth S. Vecchio*

*University of California, San Diego, La Jolla, CA 92093, +New Mexico Institute of Mining and Technology, Socorro, New Mexico 87801.

Niobium, molybdenum, and titanium silicides were synthesized by the passage of high-amplitude shock waves through elemental powder mixtures. These shock waves were generated by planar parallel impact of explosively-accelerated flyer plates on momentum-trapped capsules containing the powders. Impacts were conducted at two velocities (1.2 and 1.9 km/s) and two temperatures (~300 and ~773 K). Recovery of the specimens revealed unreacted, partially-reacted, and fully-reacted regions, in accord with shock energy levels experienced by the powder. Characterization of the partially- and fully-reacted regions for the Nb-Si system revealed only equilibrium phases: $NbSi_2$ and Nb_5Si_3. At the local particle level, the reaction kinetics can be rationalized through the production of a liquid-phase reaction product ($NbSi_2$), the formation of spherical nodules (~2um diameter) of this product through interfacial tension and their subsequent solidification (in times of 1-5 ns).

Keywords: shock-synthesis, silicides, partially-reacted.

1. INTRODUCTION

Shock-induced reactions have been studied since the 1960's but are still poorly understood. They are quite distinct from shock-induced phase transformations, such as the transformation of graphite to diamond. Shock-induced reactions also differ from detonations in that only condensed products are formed. Shock-induced reactions are closely related to combustion synthesis, and occur in the same systems that undergo exothermic gasless combustion reactions. The thermite reaction ($Fe_2O_3 + Al \rightarrow Fe + Al_2O_3$) is prototypical of this class of reactions. The first report of shock-induced reactions is due to Deribas, Batsanov, and co-workers [1]. This initial discovery was followed by activity in Japan [e.g. 2, 3], the USSR [e.g. 4-7], and the U.S.[e.g. 8-12].

Shock synthesis of compounds from powders occurs because of the extraordinarily high energy deposition rate at the surfaces of the powders, thereby changing their configuration, forcing them in close contact, activating them by introducing large densities of defects, and heating them. Some fundamental questions regarding these reactions remain unanswered. Prominent among them is the following: (1) How can the extraordinarily high reaction rates encountered in shock compression be explained? (2) Are the phases formed under shock-synthesis conditions unique and/or non-equilibrium?

This paper presents experimental results coupled with characterization and analysis that is directed at providing an answer to these questions. It is shown that the mechanism of shock-induced reaction in several silicides systems is quite different than conventional solid-state reaction mechanisms

2. EXPERIMENTAL PROCEDURES

Three elemental powder mixtures were used in this investigation: Nb-Si, Mo-Si, and Ti-Si. The base characteristics of the powders are given in Table 1. These powders had sizes smaller than 40μm (-325 mesh) and were mixed in the proportions to provide, upon reaction, the intermetallic compounds $NbSi_2$, $MoSi_2$, and Ti_5Si_3. These powders were encapsulated under controlled atmosphere in stainless steel capsules (internal dimensions of 15 mm diameter and 5 mm height). These capsules were subjected to shock compression in a Sawaoka fixture. This fixture is described in detail elsewhere [12, 13]. The system (cross-section) is shown in Figure 1. Impact velocities of 1.2 and 1.9 km/s were achieved by varying the quantity and type of explosive accelerating the flyer plate. Shock experiments were also conducted on capsules preheated to 773K.

Table I Relevent properties of constituent elements of powders

Property	Materials			
	Nb	Mo	Ti	Si
Melting Point (K)	2740	2890	1943	1685
Thermal Conductivity (W/cm K)	0.54	1.38	0.22	1.49
Heat Capacity (Cp) $a+b\,10^{-3}T+c\,10^{5}T^{-2}$ (cal/deg mole)	a 5.885 b 0.81 c - 2.2	a 5.77 b 0.28	a 5.28 b 6.91	a 5.72 b 0.59 c - 0.99
Latent Heat of Fusion (cal/g)	68	69	100	430
Compressive Strength (MPa)	200-400	300		90
Main Products with Si	$NbSi_2$	$MoSi_2$	Ti_5Si_3	
Melting Point (K)	2420	2300	2390	
Heat of Reaction (kJ/mole)	138	129.6	579.8	

After shock processing, the capsules were sectioned and analyzed by light optical microscopy, and scanning and transmission electron microscopy. The pressure and temperatures induced by shock waves in the capsules were obtained from computer simulations, conducted by Norwood and Graham [14]. Two-dimensional effects are very important since the shock waves travel faster in the capsule than in the powder. Thus, the shock waves enter the capsules laterally, as well as at their top surface, generating highly inhomogeneous pressure and temperature regimes. This inhomogeneity was markedly reflected in different regions within the recovered capsules, and was actually a highly useful effect, since it enabled the analysis of unreacted, partially-reacted, and fully-reacted regions within the same specimen.

Static reaction experiments were conducted by annealing Nb-Si diffusion couples for different times at 1200°C and recovering the specimens for observation. The reaction products and thicknesses of the reaction layers in these diffusion couples were established.

3. EXPERIMENTAL RESULTS AND CHARACTERIZATION

Shock Recovery Experiments

Figure 2 shows maps of the cross-sections for the recovered capsules for the Nb-Si and Mo-Si systems. Fully-reacted, partially-reacted, and unreacted regions are evident. Upon recovery the specimens were considerably cracked, and portions of the specimens were lost during sectioning. For the Ti-Si system, the 1.2 km/s, room temperature experiment produced full reaction, and the capsules of the other two experiments (ie. higher velocity and elevated temperature) burst, with total ejection of the synthesized material. Table 1 shows the heats of reaction for the three systems revealing the much higher heat of reaction for the Ti-Si system. The highly energetic reaction in the Ti-Si system, coupled with the shock-wave convergence along the axis of the disk, resulted in the perforation of the capsule.

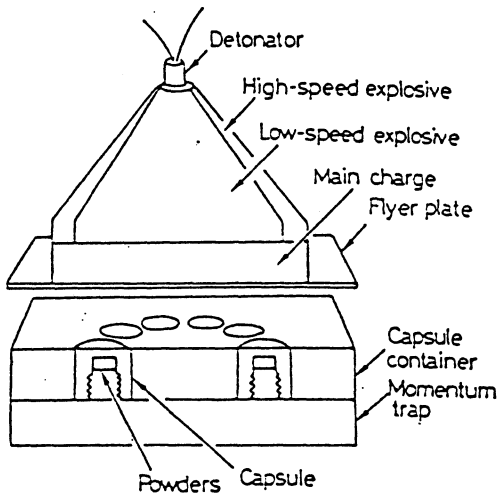

Figure 1. Schematic illustration of planar impact (Sawaoka) system.

Scanning electron micrographs of polished sections from the unreacted and fully-reacted regions in the Nb-Si system are shown in Fig. 3(a) and 3(b), respectively. In the unreacted region, the niobium particles retain their shape, while the silicon particles seem to have undergone intense plastic deformation. This is consistent with the greater mechanical strength of niobium compared with silicon. The fully-reacted regions for the Nb-Si, Mo-Si, and Ti-Si were essentially identical. Voids were present throughout, resulting from either solidification shrinkage, gases evolved during the reaction, or tensile stresses imposed on the compact prior to solidification. The presence of spherical voids, as well as dendritic structures

(a)
Impact Velocity 1.9 km/s at Room Temp.

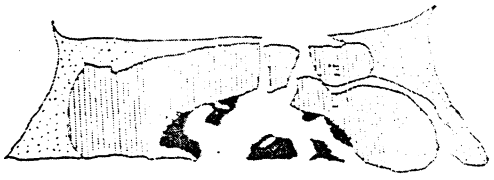

(b)
Impact Velocity 1.2 km/s at Room Temp.

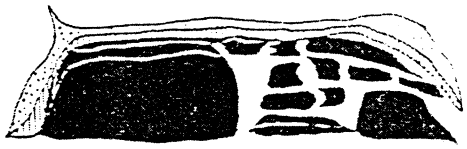

(c)
Impact Velocity 1.2 km/s at 500° C

a

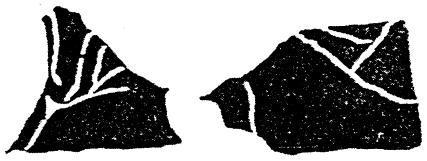

(a)
Impact Velocity 1.9 km/s at Room Temp.

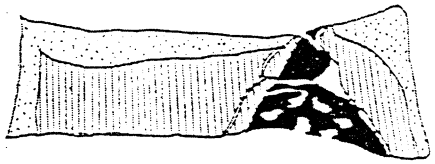

(b)
Impact Velocity 1.2 km/s at Room Temp.

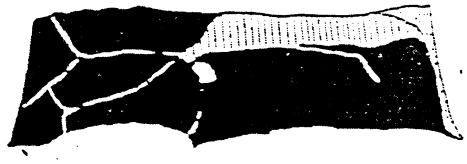

(c)
Impact Velocity 1.2 km/s at 500° C

b

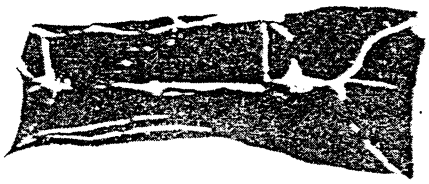

Impact Velocity 1.2 km/s at Room Temp.

c

Figure 2. Maps showing fully-reacted, partially-reacted, and unreacted regions for (a) Nb-Si system; (b) Mo-Si system; (c) Ti-Si system. Impact velocity and temperature marked on the side of each plot. Black regions represent fully-reacted, hatched regions-partially-reacted, dotted region-unreacted, and white-voids.

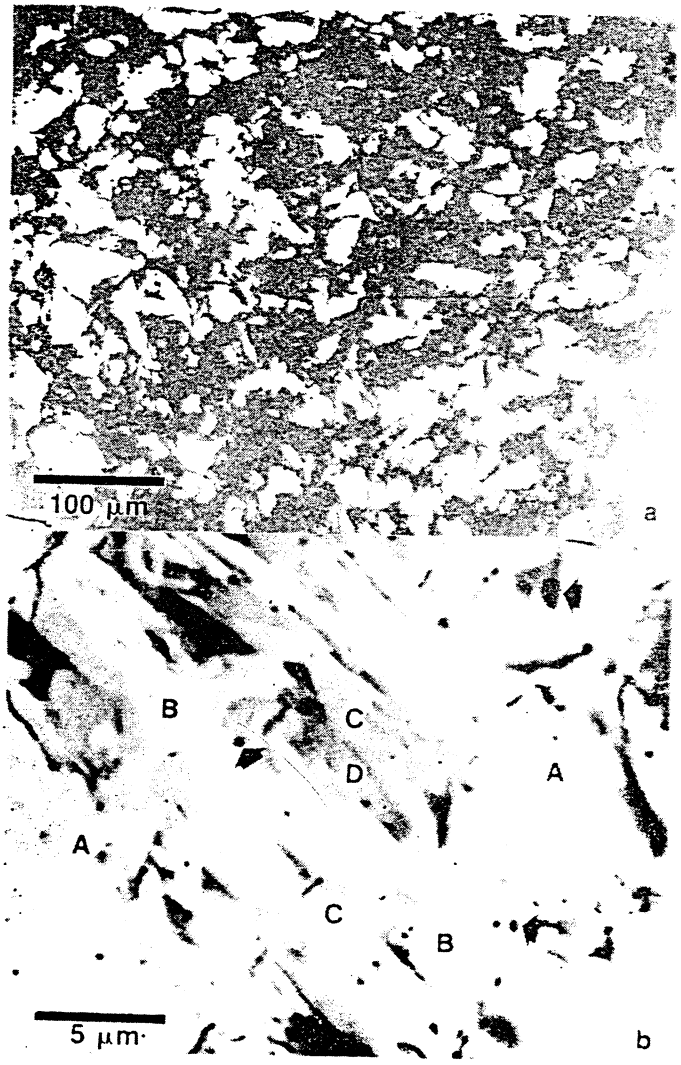

Figure 3. SEM micrographs of (a) unreacted and (b) fully-reacted regions from Nb-Si system. In (b) A-D indicated separate phases, & arrows voids.

observed are evidence of melting and re-solidification. In Figure 3b the microvoids are marked by arrows. and several different phases are present. Energy dispersive X-ray analysis of these distinct phases (marked A, B, C and D) reveals Fe, Ni, and Cr peaks, in addition to differences in the relative intensities of the much larger Nb and Si peaks. The presence of Fe, Ni, and Cr is evidence for melting of the capsule (which is stainless steel) and subsequent contamination of specimen. This is a post-shock effect, since there would be no time for diffusion of these elements during shock-wave passage.

The morphologies of the partially-reacted regions in the Nb-Si and Mo-Si systems have unique features that are indicative of the mechanisms operating. The micrographs in Figure 4 of the partially-reacted regions in the shocked samples typifies the configuration of the reacting species, (Nb or Mo, and Si) and reaction products (primarily, $NbSi_2$ or $MoSi_2$). The dark phase is silicon; profuse spheroidal nodules (grey regions) dispersed in silicon are $NbSi_2$ or $MoSi_2$. The lighter phase is niobium (Fig. 4a) or molybdenum (Fig. 4b). Careful examination of a $NbSi_2$ particle attached to niobium at high magnification revealed a very thin layer of Nb_5Si_3 between $NbSi_2$ and Nb. The profuse presence of $NbSi_2$ and $MoSi_2$ nodules at the Nb-Si and Mo-Si interfaces, and, more importantly, interspersed in the silicon are a unique aspect of shock-induced chemical reactions. Diffusion couples of pure Nb and Si annealed at 1200°C in a furnace yield a radically different reaction product morphology (see Figure 5).

Transmission electron microscopy of the partially-reacted region reveals the structure of the nodules and of the surrounding silicon matrix (Figure 6). The nodules are approximately 1-2μm in diameter and have facets. They are monocrystalline, and do not show any marked internal features, such as dislocations, stacking faults, or twins. The silicon surrounding these reacted regions shows an annealed structure with a profusion of annealing twins. A few silicon regions exhibit a microcrystalline structure as shown in Figure 7. This region either was subjected to intense plastic deformation and recrystallized (statically or dynamically) or was molten and rapidly re-solidified. This microstructure is in stark contrast with the previous silicon

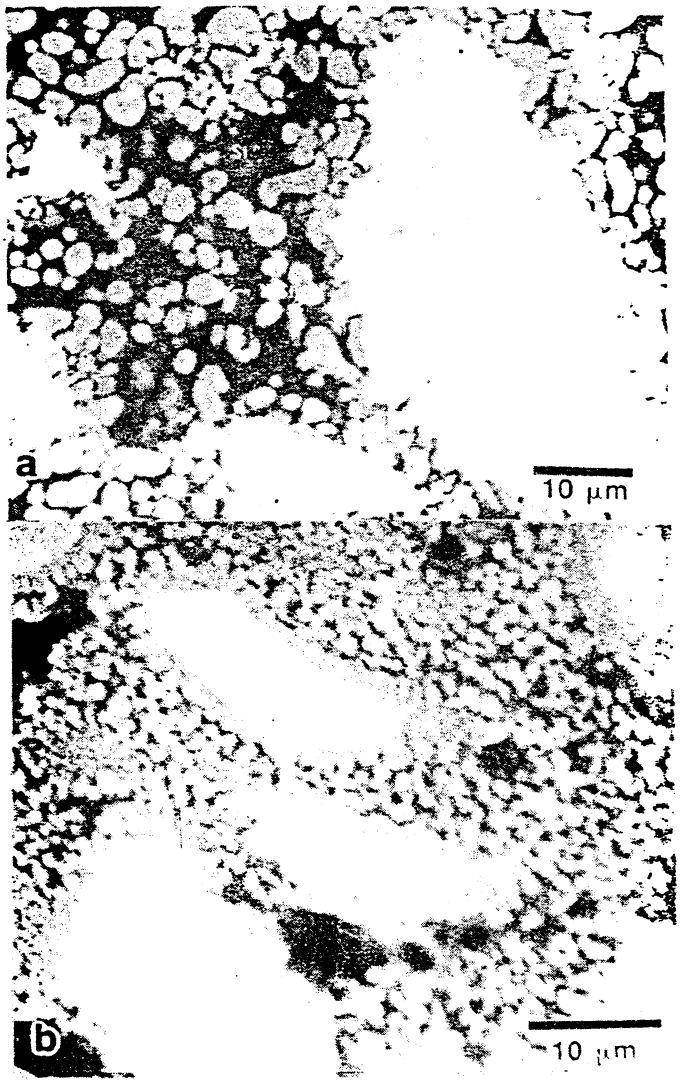

Figure 4. Partially reacted regions in (a) Nb-Si and (b) Mo-Si systems.

regions which suggested melting followed by slow re-solidification. Incontrovertible proof that silicon was molten in the partially-reacted region is provided by the observation of a fine eutectic structure present within the silicon consists of $NbSi_2$ lamellar and Si. This eutectic structure formed last as the molten, Nb-enriched silicon solidified.

Static Synthesis (Diffusion Couple) Experiments

In order to assess the kinetics of reaction under conventional heat treatment, in the solid state, pieces of niobium and silicon were polished flat, clamped together, and then encapsulated. These diffusion couples were

annealed at 1200°C for different times, sectioned, and analyzed. Figure 5 shows typical reaction layers that formed as a result of solid-state diffusion (in this example the couple was annealed at 1200°C for 2 hours). The thicknesses of the product layers as a function of time are plotted in Figure 8. The data can be easily rationalized in terms of a simple diffusion equation:

$$\chi = k\sqrt{Dt} \qquad (1)$$

where χ is the thickness of the reaction layer, D is the diffusion coefficient, t is the time, and k is a parameter that is a function of the geometry, phases formed, etc. The activation energy for diffusion for these materials varies from 200 to 400 kJ/mole. Taking an average (among the available data) between the activation energies for self-diffusion of silicon and niobium, a value of 350 kJ/mole is obtained. Hence,

$$\chi = kD_0^{1/2}\left(e^{-\Delta Q/RT}t\right)^{1/2} \qquad (2).$$

By grouping the two unknown parameters k and $D_0^{1/2}$ and fitting Eqn. 1 to the experimental results of Fig. 8, it is possible to obtain reaction layer thicknesses as a function of time for both Nb_5Si_3 and $NbSi_2$. These predicted thicknesses, for a range of temperatures below the melting point of silicon, are shown in Fig. 9. The effect of

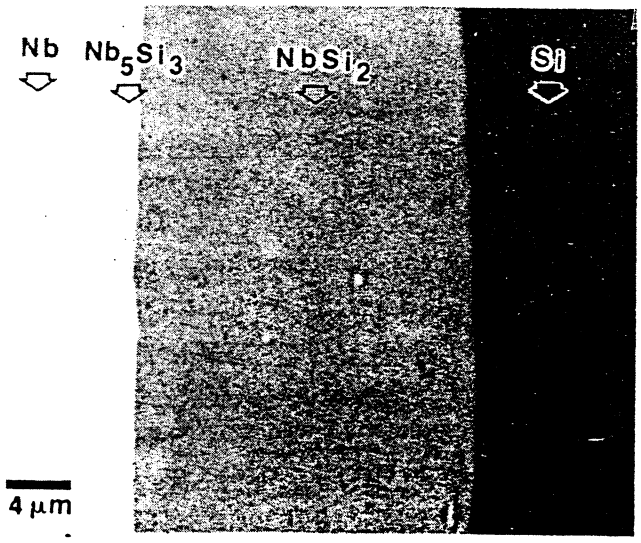

Figure 5, SEM micrographs of Nb-Si diffusion couples annealed at 1200°C for 2 hours.

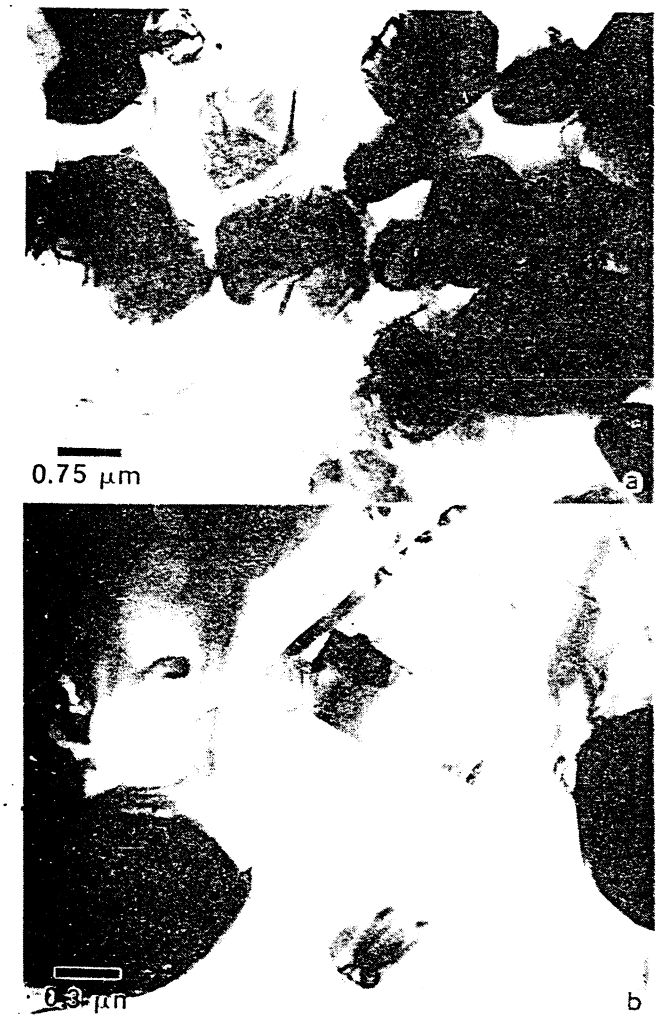

Figure 6. TEM micrographs of partially-reacted region showing (a) monocrystalline structure $NbSi_2$ and (b) annealing twins in silicon matrix.

Figure 7. Microcrystalline silicon region found in Nb-Si.

temperature on the product layer thickness is very small, in the logarithmic scale of Figure 9. The predicted reaction layer thicknesses, for a time of 5μs (maximum duration of stress pulse within shocked specimens) and a temperature of 1400°C (maximum admissible temperature for solid-state process; $[MP]_{Si}$ = 1685K) are 10^{-7} and 10^{-9}μm for $NbSi_2$ and Nb_5Si_3, respectively.

Under shock conditions the reaction front advances by a dimension on the order of the radius of the particle (~1μm) within this same time span (5μs). Thus, the reaction rates under shock conditions are 10^7 - 10^9 times higher than under static, solid-solid conditions.

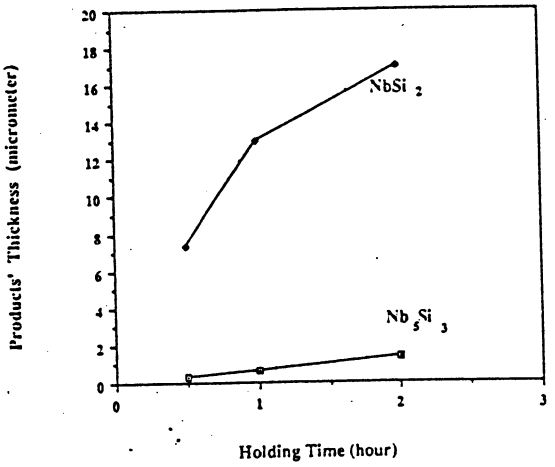

Figure 8 Thickness of $NbSi_2$ and Nb_5Si_3 reaction layers as a function of annealing time at 1200°C.

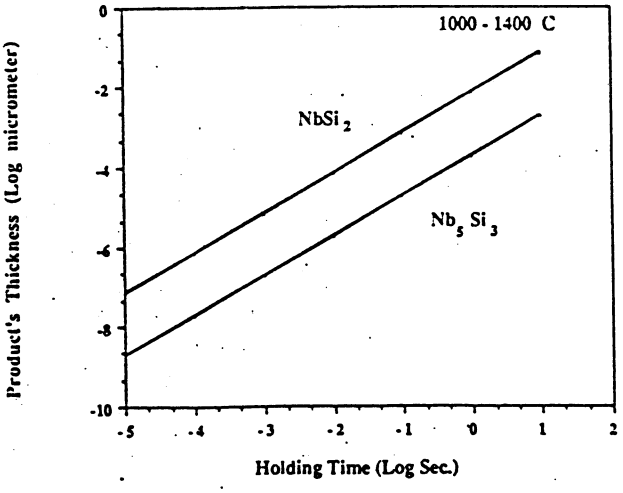

Figure 9 Predicted reaction layer thicknesses for $NbSi_2$ and Nb_5Si_3 as a function of time for temperature between 1000 and 1400°C.

Reaction Mechanism

The analysis of the partially-reacted regions in the Nb-Si shock experiments revealed the detailed nature of the reaction sequence and mechanisms. The preponderance of small $NbSi_2$ particles surrounded by silicon, as well as the existence of $NbSi_2$ particles attached to the niobium particles (Figures 4 and 5) are evidence for a reaction mechanism in which the $NbSi_2$ or $MoSi_2$ particles are continuously being generated at the interface and ejected into the (molten) silicon. Thus, no permanent diffusion barrier that would slow down the reaction process is formed, and reaction can proceed at a constant rate until the entire niobium or silicon are consumed. The simple calculation below shows that the temperature rise due to the reaction leads to a temperature (locally) higher than the melting point of $NbSi_2$. Figure 10 shows the sequence of events envisaged to occur. $NbSi_2$ will form at a Nb-Si interface, where silicon is molten and niobium is solid. Assuming an adiabatic reaction, the temperature is:

$$T = T_{MP}^{Si} + \frac{\Delta H_r}{C_p} \qquad (3)$$

The enthalpy of reaction of $NbSi_2$ is equal to 926J/g (at P = 0). The heat capacity of $NbSi_2$ was estimated by interpolation between those of Nb and Si on a mass basis (m^{Si} and m^{Nb} are mass fractions of Si and Nb):

$$C_p = m^{Si}C_p^{Si} + m^{Nb}C_p^{Nb} = 0.58 \text{ J/gK}$$

Thus, assuming that the pressure exerted by the shock wave corresponds to the threshold energy, with the melting point of silicon taken to be 1685K, a reaction temperature of T = 3,280K would be achieved. This temperature is considerably higher than the melting point of $NbSi_2$ (2,420 K, at P = 0). It is therefore possible that a sequence such as shown in Figure 11 may occur. The shock-induced reaction is initiated at (a), along the Nb-Si interface. After reaction has proceeded to a certain extent (b), surface (interfacial) forces become dominant, and the liquid reaction product agglomerates, forming a spherule (c). At this point, reaction kinetics are drastically decreased, due to the reduction in the Nb-Si interfacial area, and solidification of the sphere starts (d). As the sphere solidifies, new nuclei

form along the Nb-Si interface (e). The new nuclei grow, agglomerate into spheres when they reach a critical size, and form neighboring spheres (f). As these neighboring spheres solidify, they exert forces on the first sphere, expelling it (g) and thus exposing fresh surfaces. This reaction process can continue unimpeded, until the reactants are consumed.

Turbulent flow of liquid silicon under shock can also contribute to the detachment of the spherules from the interface. The interfacial energies of silicon and $NbSi_2$ are not known, but it is possible to estimate them from the surface energies of liquid Si and Nb:

$$\gamma_S^{Nb} = 1900 \text{ ergs/cm}^2 \text{ at } 2473°C$$
$$\gamma_S^{Si} = 730 \text{ ergs/cm}^2.$$

By interpolation on a mass fraction basis:

$$\gamma_S^{NbSi_2} = m^{Si}\gamma_S^{Si_2} + m^{Nb}\gamma_S^{Nb} = 1455 \text{ ergs/cm}^2.$$

Thus, the formation of $NbSi_2$ spherules from a continuous liquid layer of $NbSi_2$ leads to an overall decrease in energy. The cooling rate of the $NbSi_2$ spherules can also be calculated. Equation 4 shows the effect of time, t, and distance r, on temperature, T, for a spherical particle (spherical coordinates):

$$\frac{\partial T}{\partial t} = \frac{k}{\rho C}\left(\frac{\partial^2 T}{\partial r^2} + \frac{2}{r}\frac{\partial T}{\partial r}\right) \qquad (4)$$

where k, ρ, and C are the thermal conductivity, density, and heat capacity, respectively. The initial conditions are:

$$T = 3{,}200 \text{ K at } t = 0 \text{ for } r < a$$
$$T = 1{,}600 \text{ K at } t = 0 \text{ for } r > a.$$

where "a" is the radius of the nodule, which can be obtained from measurements in Figures 4 and 5; an average value of 1μm was taken for the calculations. Values for k, ρ, and C were averaged from Nb and Si for $NbSi_2$. Figure 11 shows the results of the computations using Eqn. 4. The three-dimensional plot shows the effects of time, in nanoseconds) and temperature (in Kelvin) on the size of $NbSi_2$ nodules; the solidification heat is not incorporated into the calculations. Nevertheless, it is clearly seen by the

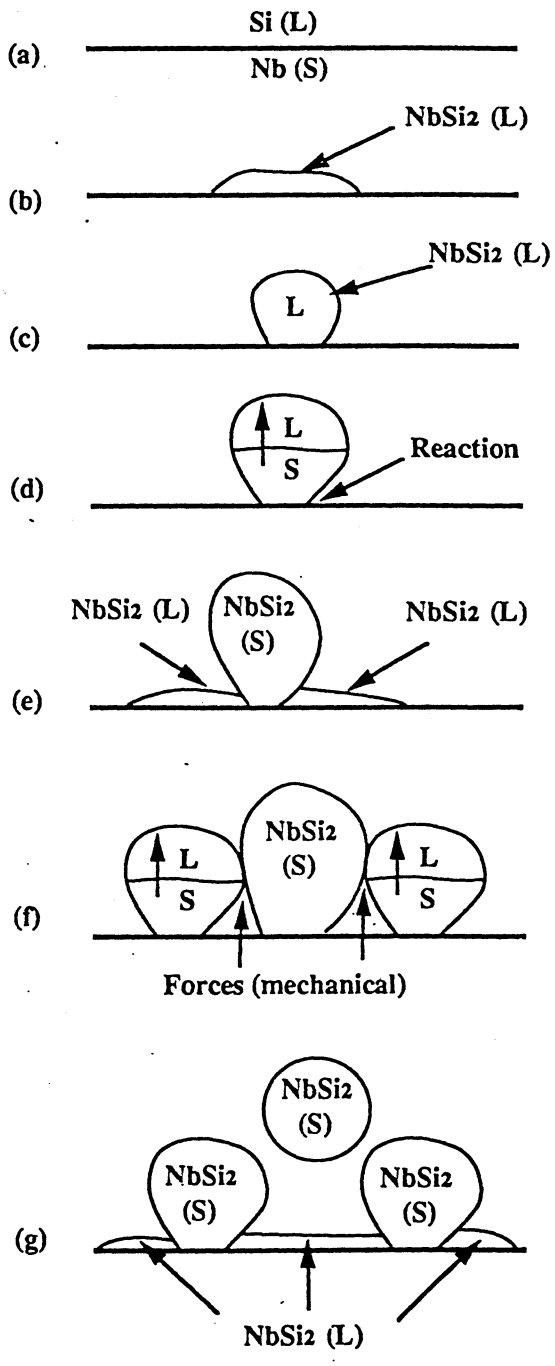

Figure 10. Sequence of events in the synthesis of $NbSi_2$ spherules at Nb(solid)-Si(liquid) interface under shock loading; (a) and (b) nucleation and growth of thin layer; (c) interfacial energy produces spheroidization; (d) solidification and reduced reaction; (e) adjacent reaction regions form in newly exposed interface; (f) spheroidization and solidification of adjacent reaction region; (g) expulsion of spherule.

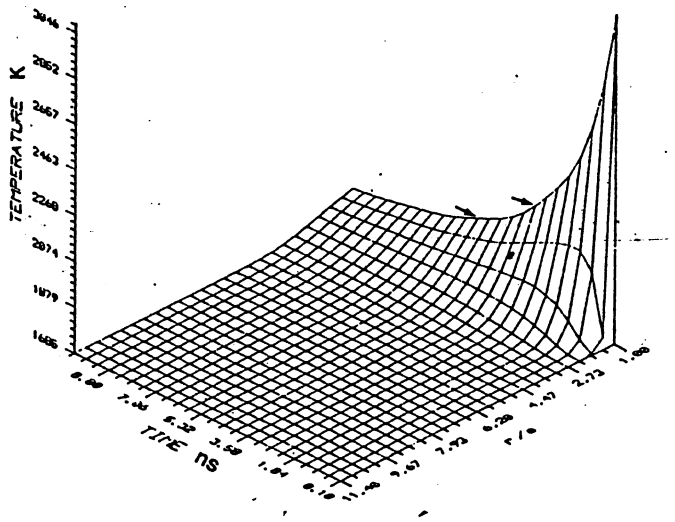

Figure 11 Predicted heat extraction from Eqn. 4 for spherule with initial temperature of 3200 K while surroundings are at 1600 K. Arrows indicate temperatures at 2 and 5ns cooling times.

time, that solidification can be initiated 2-5ns after the spherule is formed. Thus, the solidification time is a small fraction (~1/1000) of the shock pulse duration time. It is therefore easy to see how successive generations of nodules can be formed, solidified, and ejected from the reaction interface.

4. CONCLUSIONS

1. It was possible to successfully initiate and propagate shock-induced reaction for the three systems investigated, and the extent of reaction was found to increase with shock energy, temperature, and energy of reaction.
2. The following qualitative statements can be made: (a) as the heat of reaction increases, the pressure/temperature necessary for full reaction decreases, (b) the extent of shock-induced reaction increases with impact velocity, at a constant temperature, and with temperature, at a constant impact velocity.
3. Electron microscopy observations reveal that the main reaction product in the partially-reacted regions is $NbSi_2$, formed as spherules with radii of approximately 1μm. These spherules are formed at the Nb-Si interface and are expelled into the silicon.
4. There is clear indication that silicon melting is a prerequisite for shock-induced reactions.
5. The reaction kinetics in static solid-state reactions were established and found to be lower, by ~10^8, to the kinetics in shock compression.
6. A reaction mechanism occurring at the metal-Si interface is proposed involving the dissolution of (Nb, Mo, Ti) into molten Si, the reaction producing the molten intermetallic, its spheroidization, solidification, and subsequent expulsion into liquid silicon melt. In this reaction mechanism a fresh solid (Nb, Mo,or Ti)-liquid (Si) interface is continuously maintained, enabling a high reaction rate.

References

1. S. S. Batsanov, A. A. Deribas, E. V. Dulepov, M. G. Ermakov, and V. M. Kudinov, *Comb. Expl. Shock Waves USSR*, **1**, 47 (1965).
2. Y. Horiguchu and Y. Nomura, *Carbon* **2**, (1965) 436.
3. Y. Horiguchu and Y. Nomura, *Chem. Industry London*, Oct. (1965) 1791.
4. G. A. Adadurov, V. I. Gold'anskii, and P. A. Yampol'skii, *Mandeleev Chem. J.*, **18** (1973) 92..
5. G. A. Adadurov, and V. I. Gold'anskii, *Russian Chemical Rev.*, **50** (1981) 948..
6. A. N. Dremin and O. N. Breusov, *Russian Chem. Rev.*, **37** (1968) 392.
7. S. S. Batsanov, *Russian Chem. Rev.*, **37** (1968) 197.
8. R. Graham, B. Morosin, E. L. Venturim, and M. J. Carr, *Ann. Rev. Mater. Sci.*, **16** (1986) 315.
9. B. Krueger, A. Mutz, and T. Vreeland, Jr., *J. Appl. Phys.*, submitted for publication, (1991).
10. Y. Horie and M. J. Kipp, *J. Appl. Phys.*, **63** (1988) 5718.
11. M. B. Boslough, *J. Chem. Phys.*, **92** (1989) 1839.
12. L. H. Yu, and M. A. Meyers, *J. Matls. Sci.*, **26** (1991) 601.
13. A. B. Sawaoka and T. Akashi, U. S. Patent 4655830 (1987).
14. F. R. Norwood and R. A. Graham, in "Shock-waves and High-Strain-Rate Phenomena in Materials," M. Dekker, 1991, in press.